Effect of Conformation and Combination of 1,3-Bis(4-pyridylthio)propan-2-one upon Coordination Architectures: Syntheses, Characterizations and Properties

Benlai Wu,[a] Daqiang Yuan,[a] Feilong Jiang,[a] Lei Han,[a] Benyong Lou,[a] Caiping Liu,[a] and Maochun Hong*[a]

Keywords: Coordination polymer / Interpenetration / Conformation analysis / Magnetic property / Fluorescence

Self-assemblies of the conformationally labile ditopic ligand 1,3-bis(4-pyridylthio)propan-2-one (L) with square-planer nodes Co^{II}, Ni^{II} and with linear nodes Ag^{I} have afforded three new coordination polymers, $\{[Ni(L)_2Cl_2]\}_\infty$ (**1**), $\{[Co(L)_2(SCN)_2]\cdot(DMF)_2\}_\infty$ (**2**) and $\{[AgL]NO_3\}_\infty$ (**3**), respectively. Structural analyses of these polymers and conformational analyses of L have revealed that metal-assisted conformational selectivity and unique combinations of conformational isomers of L around the metal nodes probably play the key role in determining the structural topologies. In **1**, a C_2 symmetric array of two sorts of conformational isomers of L around Ni^{II} centers results in a 3D interpenetrating framework, while in **2** a combination of two types of conformational isomers of L around the inversion center Co^{II} provides a 3D interpenetrating architecture of $CdSO_4$-like topology. In **3**, L presents only a typical conformation, with higher steric energy, that links linear nodes Ag^{I}, leading to a 1D U-like chain. The magnetic properties of **1** and **2**, as well as the interesting fluorescent properties of **3**, have also been investigated.

Introduction

Flexible ditopic or multitopic organic ligands that encode more variable chemical information, such as their flexibility and conformational freedoms, have attracted increasing interest in crystal engineering.[1–11] A combination of selective metal ions with tailored flexible ligands is very fruitful in building a large assortment of coordination polymers with unique architectures,[12–19] sometimes with interpenetrations[20–24] and interesting material properties.[25–29] Moreover, some conformational isomers of a flexible ligand in solution may be induced, enhanced, recognized and stabilized by numerous factors, especially by metal coordination preferences in a self-assembly process, providing additional opportunities to design and build unique coordination motifs as well as to separate an unfavorable conformation. This is clearly highlighted by Stang's rational design based on the conformationally defined dihedral angle of 4,4′-dithiodipyridine,[30] although such cases are still comparatively rare.

Recently, we have concentrated on the coordination chemistry of flexible ligands, particularly on metal-based supramolecular architectures of N-containing heterocyclic thioethers with various arene bridges, and have obtained several unique structural motifs.[31–34] While this work was in progress several reports of new Ag^{I} polymers coordinated by related N-containing heterocyclic thioethers with alkane bridges appeared.[35,36] Pursuing our work in this area, we deliberately designed dithioether ligand 1,3-bis(4-pyridylthio)propan-2-one (L) (Scheme 1). The advantages of this ligand are (i) as arene bridges are displaced by propan-2-one groups, the conformational transformation barrier is so low that some conformations of L may be induced by weak forces, such as solvent and electrostatic effects, and recognized by metal-coordination and further stabilized in crystallization; (ii) the relative rigidity resulting from the permanent planar requirement of the propan-2-one group, needed for sp^2 hybridization of its central carbon, enlarges conformational otherness, resultining in differences from analogs with simple alkane bridges; (iii) incorporating the ketone group into the alkane chain endows the ligand with a hydrogen-bond receptor, which will functionalize the resultant architecture. Consequently, using L to assemble with the square-planar nodes Ni^{II} and Co^{II} in solvothermal methanol or DMF/diethyl ether systems, we were able to prepare two new 3D interpenetrating polymers with distinctive topologies, owing to metal-assisted conformational selectivity and unique combinations of ligand L. In contrast, the assembly of L with linear node Ag^{I} in a three-layered diffusion system produced a 1D U-like polymer, where nitrate anions template both the architecture of the polymer and the typical conformation of L. We report here the resultant structures of $\{[Ni(L)_2Cl_2]\}_\infty$ (**1**), $\{[Co(L)_2(SCN)_2]$

[a] State Key Laboratory of Structural Chemistry, Fujian Institute of the Research on the Structure of Matter, Chinese Academy of Sciences,
Fuzhou, Fujian, 350002, China
Fax: +86-591-8371-4946
E-mail: hmc@ms.fjirsm.ac.cn
Supporting information for this article is available on the WWW under http://www.eurjic.org or from the author.

 DOI: 10.1002/ejic.200400734

·$(DMF)_2\}_\infty$ (**2**) and $\{[AgL]NO_3\}_\infty$ (**3**), along with conformational analysis of L. Furthermore, we also report quantitative magnetic characterizations of complexes **1** and **2**, and the fluorescence properties of ligand L and complex **3**.

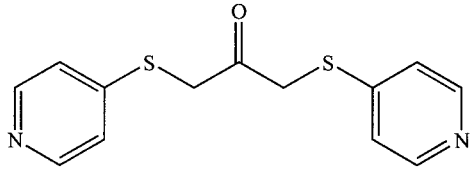

Scheme 1. Ligand L.

Results and Discussion

Synthesis and Conformational Analysis of 1,3-Bis(4-pyridylthio)propan-2-one (L)

Ligand L was prepared by the substitution reaction of 1,3-dichloro-2-propanone and sodium methylate, following the strategy we utilized previously to synthesize N-containing heterocyclic thioether ligands;[31–34] however, the separation of L from the oil phase was a key problem. Ultimately, the pure solid-phase of L was obtained through subtle use of its temperature-dependent solubility in water in the separation and purification process.

Propan-2-one is a planar molecule that shows no conformation due to sp^2 hybridization of its central carbon atom. However, as sulfur atoms are introduced at the 1 and 3 carbon atoms, the substituted compound displays three typical conformations, namely A, B and C isomers. In addition, as two 4-pyridyl groups are bound to the two sulfur atoms, three typical conformational isomers are expected, e.g. A1, A2 and A3 of conformation A (Scheme 2). Thus the resulting ligand L can adopt many conformational isomers. Generally, these conformational isomers will be balanced in solution due to their lower steric and larger solvation energy. Among them, five types of conformational isomers of L were obtained through assembly of L with tailored metal nodes (Scheme 2). The common feature of isomers A1, A2 and A3 is that the two sulfur atoms linked to propan-2-one group are almost coplanar with propan-2-one group (namely plane SCCCS). For the A1 conformation, the two nitrogen atoms of pyridyl groups are also located in the SCCCS plane, similar to the optimized conformational isomer L_{ideal} by Gaussian 03.[37] However, the combination of two pyridyl groups at either the same or each side of the SCCCS plane will afford isomer A2 or A3, respectively. For C1 and C2 isomers, their two 4-mercaptopyridine groups bind to each side of the propan-2-one plane to form the trans conformations, but the obvious distinction shown in

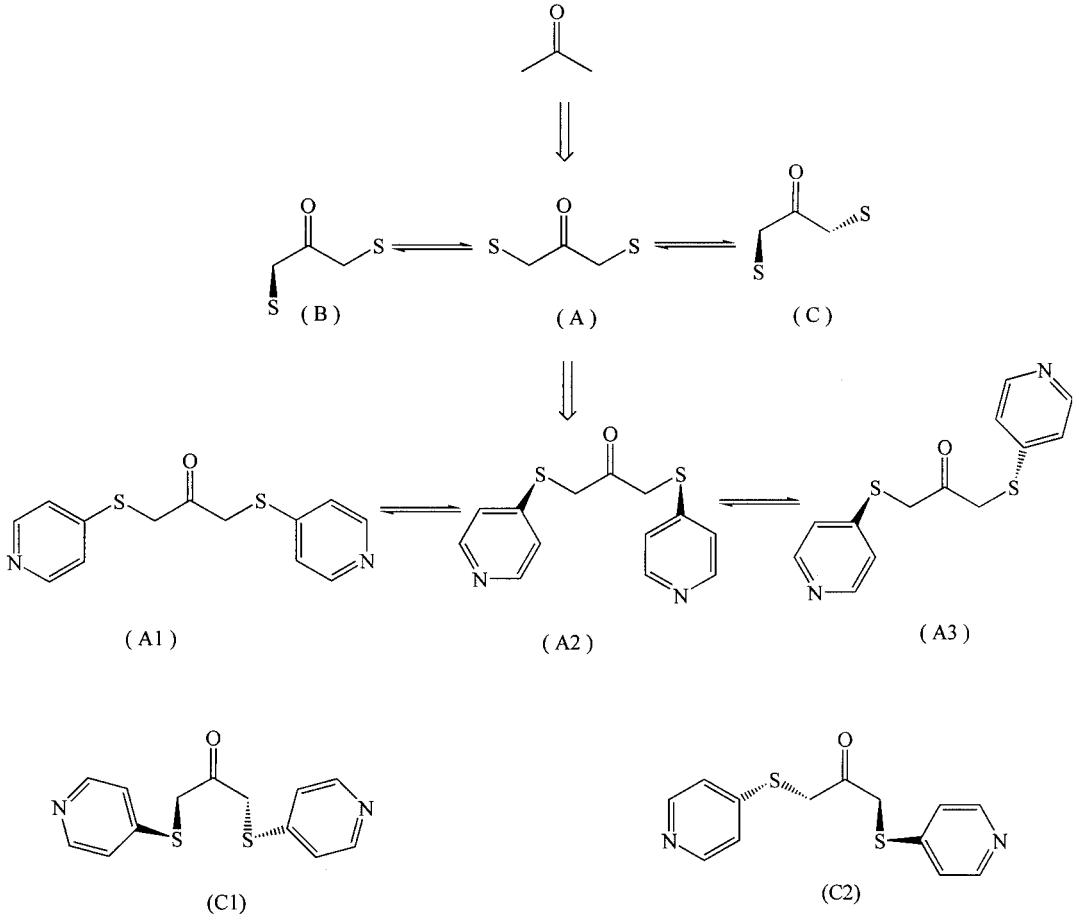

Scheme 2. Formation process of conformational isomers of L (with the A form as example) and representation of conformational isomers of ligand L obtained in its coordination complexes.

Scheme 2 defines them as different conformations. Furthermore, using Gaussian 03 we calculated quantitatively their conformational energies (Table S1). Compared with the optimized conformational isomer L_{ideal} (the energy of L_{ideal} is arbitrarily regarded as the standard of zero), their steric energies (kJ mol^{-1}) are evaluated as $E^{A1}{}_{steric}$ 400.94, $E^{A2}{}_{steric}$ 411.65, $E^{A3}{}_{steric}$ 406.01, $E^{C1}{}_{steric}$ 389.86 and $E^{C2}{}_{steric}$ 724.51. Clearly, the energy gaps between those conformational isomers range from 5 to 22 kJ mol^{-1}, except for $E^{C2}{}_{steric}$ which is notably higher due to the relatively low statistical distribution of propan-2-one groups in this L. But as we will show, metal-induced conformational isomers A1, A2, C1 and C2 and their unique combinations around metal centers may play a crucial role in pre-defining the resultant polymeric architectures.

Crystal Structures of $\{[Ni(L)_2Cl_2]\}_\infty$ (1) and $\{[Co(L)_2(SCN)_2]\cdot(DMF)_2\}_\infty$ (2)

Complex **1** was obtained from a solvothermal methanol system. An X-ray structural analysis discloses that it crystallizes in orthorhombic space group *Ibca* and is a 3D sixfold interpenetrating diamondoid framework. Each Ni^{II} center is in a distorted octahedral environment surrounded by four pyridines that occupy equatorial sites in a paddlewheel array and two Cl^- that occupy axial sites (see a in Figure 1). The Ni–N bond distances range from 2.123(8) to 2.128(8) Å and Ni–Cl is 2.398(3) Å, while the in-plane andaxis-transition angles are 179.4(3) and 179.33(17)°, respectively. The Ni^{II} centers are linked by four L and act as square-planar nodes in the network. Exo-bidentate spacers L in **1** display A1 and C1 conformational isomers, and the unique array in A1A1C1C1 form around the metal centers produces a C_2 axis that passes through the Ni^{II} center and equally bisects the equatorial plane N1–N1A–N2A–N2. Furthermore, neighboring L around the Ni1 center extend above or below the equatorial plane, resulting in the sharp deviation of binding sites N1B, N1C, N2B and N2C from the least-squares plane N1–N1A–N2A–N2–Ni1, with deviation distances of N1B, N1C, N2B and N2C from the least-squares plane of 4.98771, –4.98771, –6.0371 and 6.0371 Å, respectively. Clearly, the four nickel(II) nodes bonded by N1B, N1C, N2B and N2C atoms are expected to be at the vertexes of a distorted tetrahedron. In this manner, a 3D diamondoid framework forms (b in Figure 1), which is indicative of a distinctive difference from widely encountered 2D grids constructed by square-planar nodes with other ditopic ligands.[38–41] Adjacent $Ni^{II}\cdots Ni^{II}$ bridged by A1 and C1 are separated by 16.435 and 14.869 Å, respectively (b in Figure 1). The long spacers between coordination sites result in large cavities within the diamondoid cages. However, due to the absence of large guest molecules to fill the void space, the potential voids are filled through mutual interpenetration of five independent equivalent frameworks, generating a sixfold interpenetrating 3D architecture (c in Figure 1).

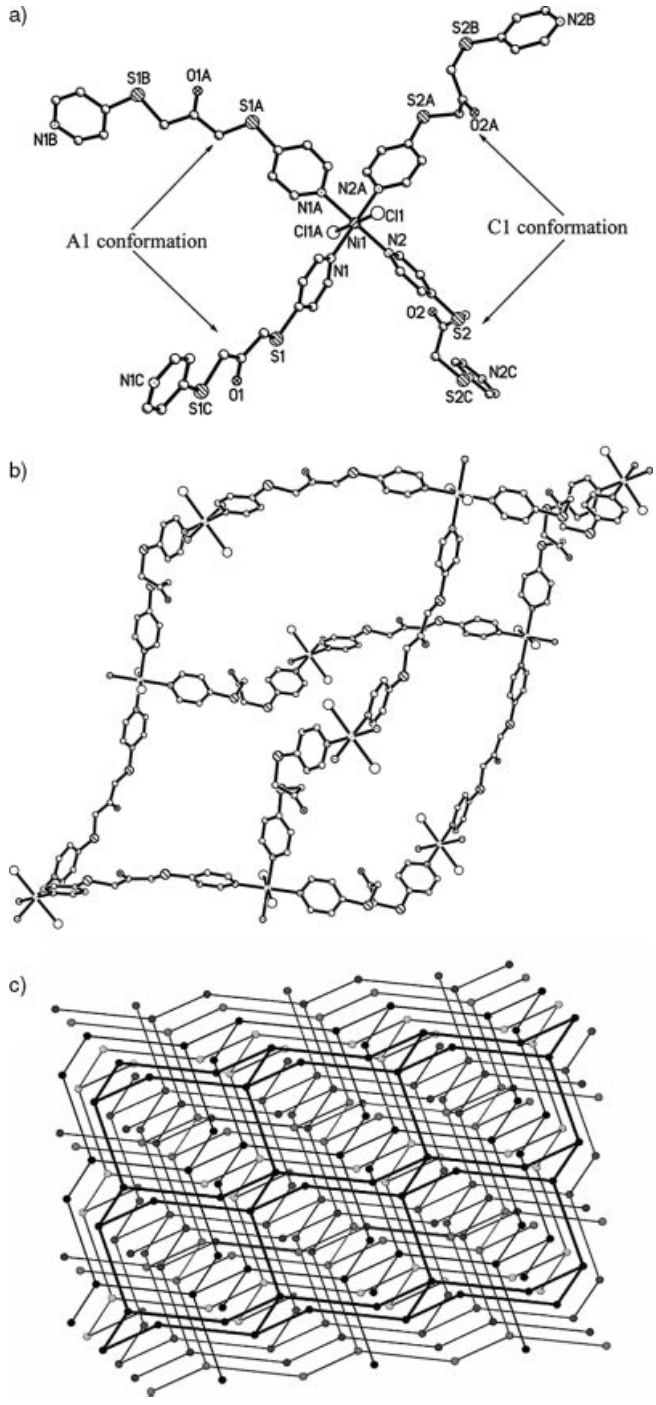

Figure 1. Views of the C_2 symmetric array of conformational isomers A1 and C1 around six-coordinate Ni^{II} centers (a), the single diamondoid cage generated through twelve L (six A1 and six C1) bridging ten Ni^{II} centers (b), and the sixfold interpenetrating diamondoid network with bridging and terminal ligands L and Cl^- omitted for clarity (c) in **1**.

Complex **2**, assembled in a DMF/diethyl ether system, crystallizes in monoclinic space group *C*2/*c* and possesses a 3D threefold interpenetrating network with $CdSO_4$-like topology. Each Co^{II} center in **2** is also in a compressed octahedral environment surrounded by four pyridines, which occupy equatorial sites, and by two SCN^- that occupy axial

sites (a in Figure 2). The Co–N bond distances range from 2.087(6) to 2.210(5) Å while the in-plane and axis-transition angles are 180.0(3) and 180.0(2)°, respectively. In complex **2**, each Co^{II} center, linked by four L, plays the role of square-planar node, in the same way as the Ni^{II} node in complex **1**. Exo-bidentate spacers L in **2**, however, display A1 and C2 conformational isomers and array in A1C2A1C2 form around the inversion center Co^{II}. Moreover, two A1 isomers bound to the Co1 center extend either above or below the least-squares plane N1–N2–N1A–N2A–Co1, with their binding sites N1B and N1C deviating sharply from the least-squares plane, by –8.1064 and 8.1064 Å, respectively. In contrast the N2B and N2C binding sites of the two C2 isomers deviate comparatively slightly from the least-squares plane, by –1.9237 and 1.9237 Å, respectively. Consequently, the architecture of **2** is completely different from that of **1** with the diamondoid framework. As clearly shown in part b of Figure 2, the combination of A1 isomers and Co^{II} nodes forms 1D undulating chains, which are further alternately connected along two perpendicular directions by the coordination of C2 isomers with Co^{II} nodes. Consequently, a 3D network with a $CdSO_4$-type topology is generated. Furthermore, the $CdSO_4$-like architecture produces large channels that have an opening of about 30.720×14.722 $Å^2$ (see b and c in Figure 2). Part d in Figure 2 shows the threefold interpenetration of $CdSO_4$-like architecture in the crystal, which effectively reduces the void space. Even so, it has a porous rather than a close-packed structure, such that DMF molecules are entrapped within it.

A combination of four-connected nodes and ditopic ligands can provide 2D grids or novel 3D nets, some interesting architectures of which have been exploited recently.[42,43] Notably, both complex **1** and **2** are 3D nets bridged by the

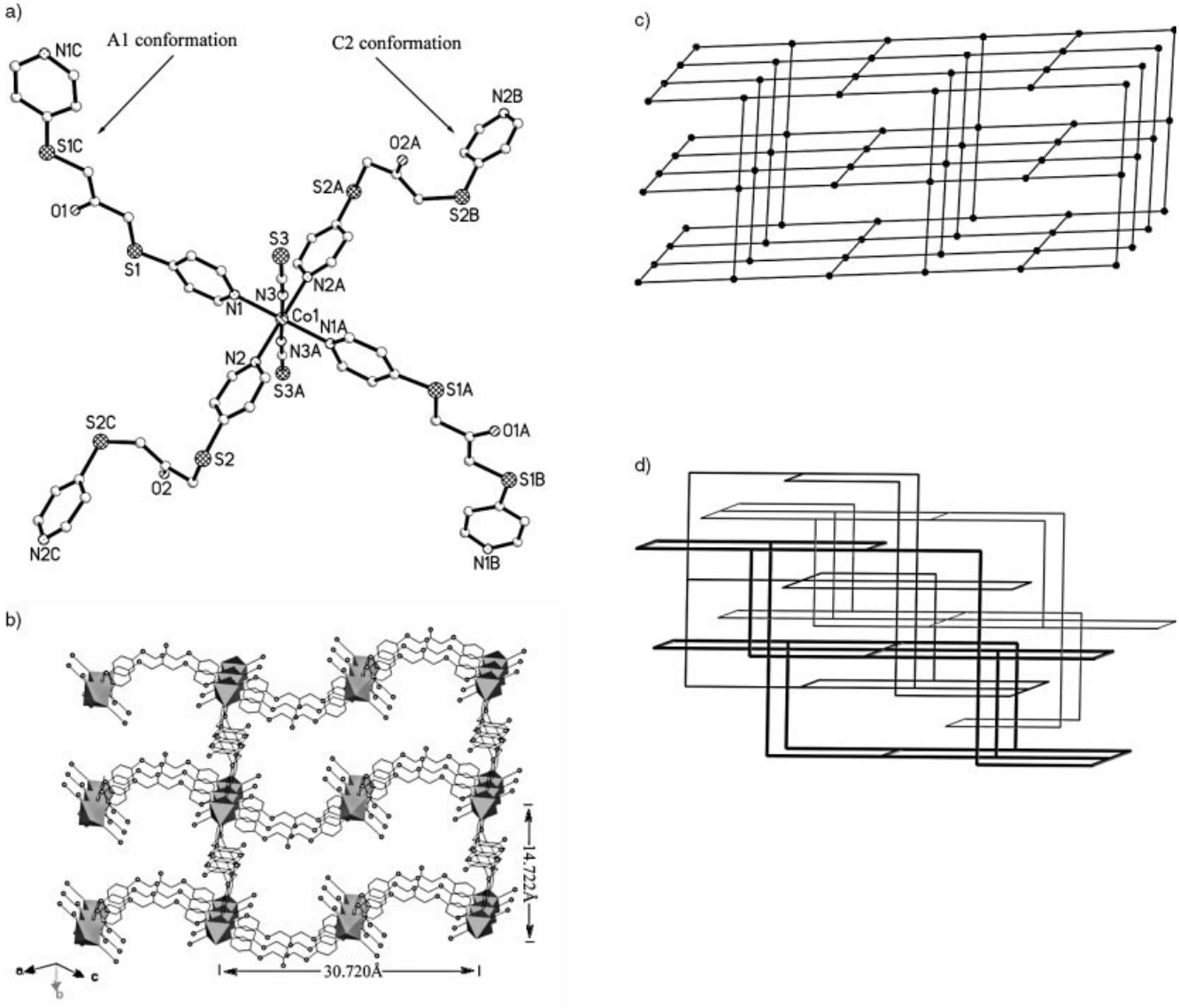

Figure 2. Combination of conformational isomers A1 and C2 around the inversion center of the six-coordinate Co^{II} (a), the 3D open framework containing large tunnels (b), schematic of the $CdSO_4$-like topology (c) and the 3D threefold interpenetrating network with bridging and terminal ligands L and SCN^- omitted for clarity (d) in **2**.

same ditopic ligands L bonded to four-connected nodes Co^{II} or Ni^{II}, but possess different topologies. Although many factors are involved, conformational isomers of L and their unique combination around metal centers, as depicted above, presumably play the key role in determining the structural topologies.

Crystal Structure of $\{[AgL]NO_3\}_\infty$ (3)

Complex **3**, obtained through a three-layered diffusion method, crystallizes in orthorhombic space group *Pnma* and possesses a 1D U-like chain architecture. The Ag^I ion in **3** shows linear coordination, in which the N1–Ag1–N1A angle is 180.0(3)° and Ag1–N1 and Ag1–N1A bond lengths are 2.151(7) Å (Figure 3). Each L, similar to other dithioether ligands containing 4-pyridyl groups in Ag^I complexes we reported previously,[34] acts as an *exo*-bidentate ligand and bridges two Ag^I centers with its two pyridyl nitrogen atoms to construct a 1D chain structure. Interestingly, L in **3** only presents an A2-typical conformation with higher steric energy than that of isomers A1 and A3. The inversion array of A2 around Ag^I centers results in the unique U-like framework, with the $Ag^I\cdots Ag^I$ distance and deep length of the "U" chain (S···S) being 7.283 and 13.365 Å, respectively, which differ from the structures found in Ag^I and N-containing heterocyclic thioethers.[34,36] Notably, nitrate ions located in "U" chains stabilize the A2-typical conformation of L through weak interactions between its oxygen atoms and Ag^I (O3···Ag1A and O3···Ag1, 2.872 Å).

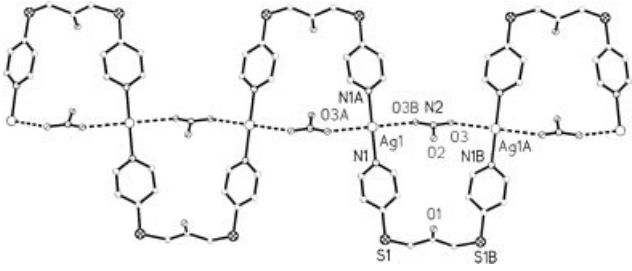

Figure 3. 1D U-like chain architecture in **3**, showing the weak interactions between the counter-anion and Ag^I as well as the template of counter-anions.

Magnetic Properties of Complexes 1 and 2

The temperature (T) dependencies of the magnetic susceptibility (χ_M) of complexes **1** and **2** were measured in the range 2–298 K under fixed fields of 5 and 10 kG, respectively; Figures 4 (see a and b) show the corresponding χ_M vs. T and μ_{eff} vs. T plots. For **1**, μ_{eff} decreases very slowly from 3.45 μ_B at 298 K to 3.29 μ_B at 8 K and then rapidly decreases to 2.53 μ_B at 2 K. The μ_{eff} of 3.45 μ_B per Ni^{II} at room temperature is larger than that calculated for the spin-only case (2.83 μ_B), revealing a significant orbital contribution, which always causes zero-field splitting. The magnetic behavior of complex **1** can be explained by large zero-field splitting, as well as a weak ferromagnetic interaction under the molecular field approximation. The best fit of Equation (1) to the data was achieved with $g = 2.31$, $D/k = 12.25$ K, $\theta = 0.94$ and $R = 4.5\times10^{-6}$ [$R = \sum(\chi_{obsd}-\chi_{cacld})^2/\sum\chi_{obsd}^2$].

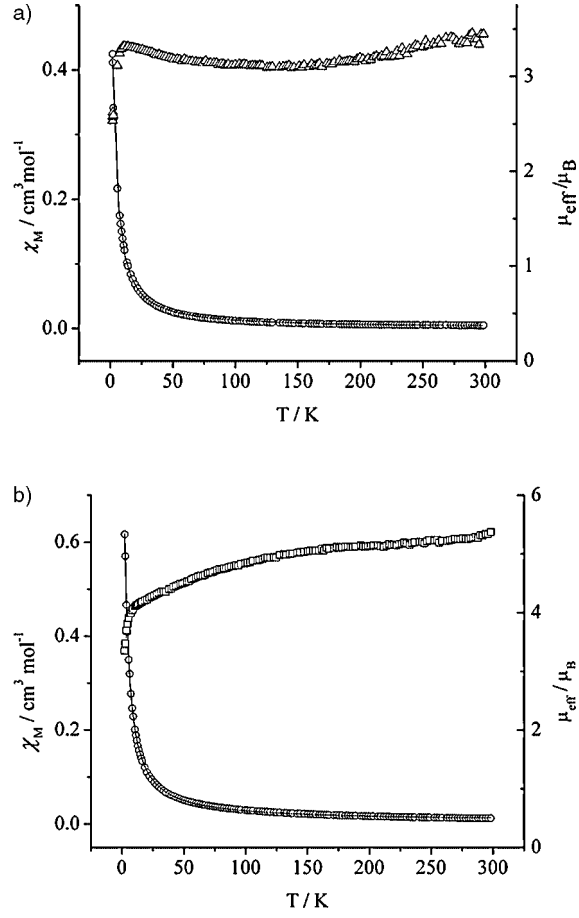

Figure 4. χ_M (○) and μ_{eff} (Δ) vs T with the theoretical fit (−) for **1** (a), and χ_M (○) and μ_{eff} (□) vs. T with the theoretical fit (−) for **2** (b).

$$\chi_M = \frac{2Ng^2\beta^2}{3k(T-\theta)}\left[\frac{2kT/D - 2kT\exp(-D/kT)/D + \exp(-D/kT)}{1+2\exp(-D/kT)}\right] \quad (1)$$

For complex **2**, the experimental μ_{eff} per Co^{II} ion at room temperature is ca. 5.38 μ_B, which is larger than that calculated for the spin-only case (3.87 μ_B), indicating a typical contribution of the orbital momentum for the $4T^1{}_g$ ground state.[44] Upon cooling, μ_{eff} gradually decreases to 4.06 μ_B at 9 K and then dramatically decreases to 3.35 μ_B at 2 K. The χ_M^{-1} vs. T plot is essentially linear, and least-squares fitting of the data to the Curie–Weiss law gives $C = 3.62$ cm^3 mol^{-1} K and $\theta = -17.50$ K. The negative value of θ may be attributed to antiferromagnetic interactions between Co^{II} ions. To date, quantitative magnetic analyses of cobalt(II) complexes have been a challenge due to the complexity of magnetic anisotropy originating from spin–orbit

coupling and axial distortion. However, when cobalt(II) ions are located in a perfect or slightly distorted octahedral ligand field, the isotropic model proves to be preferable for describing the magnetic data.[45] As indicated in the structure description, each Co^{II} center in **2** is ligated by six nitrogen atoms in a slightly distorted octahedral geometry and these metal nodes are linked by long spacers L to build a 3D $CdSO_4$-like framework. Thus, a simplified analysis of this coupling system is based on considering the exchange coupling between two adjacent paramagnetic centers in an infinite chain and interchain interaction (zJ) under the molecular field approximation. Assuming an isotropic exchange between Co^{II} ions, the magnetic susceptibility per Co^{II} ion can be expressed as:

$$\chi_M^{J+J'} = \frac{\chi_M^{J}}{1-(2zJ'\times\chi_M^{J})/N\beta^2g^2}$$

$$\chi_M^{J} = \frac{N\beta^2g^2S(S+1)}{3kT}\frac{1+u}{1-u} \quad u = \coth\left[\frac{JS(S+1)}{kT}\right]-\left[\frac{kT}{JS(S+1)}\right] \qquad (2)$$

The best fit (assuming $zJ = 0$) of the experimental data to Equation 2 yields $J = -0.36\ cm^{-1}$, $g = 2.28$, with an agreement factor $R = \sum(\chi_{obsd}-\chi_{cacld})^2/\sum\chi_{obsd}^2) = 2.0\times10^{-5}$. It seems that the spin-only model gives quite a good fit.

On the basis of the molecular structures and the magnetic calculations of complexes **1** and **2**, we conclude that the interaction via the bridge L is very weak – indicative of the long and unconjugated ligand L being unfavorable for the electronic interactions needed for efficient superexchange between paramagnetic metal centers.

Fluorescence Properties of Ligand L and Complex 3

Figure 5 depicts solid-state photoluminescent spectra of **3** and free ligand L at room temperature. Free ligand L is strongly photoluminescent and exhibits intense green emission with a single broad band at λ_{max} = 537 nm, corresponding to an excitation at λ_{max} = 370 nm. The emission properties of **3** are complicated and very interesting. Although several Ag^I polymers that emit photoluminescence at room temperature have been reported,[46–49] complex **3** shows, unusually, multiple emission bands. When excited at 365 nm, it displays two weaker blue emission bands at λ_{max} = 416 and 442 nm and one stronger, broad, green emission band at λ_{max} = 541 nm. The low-energy band of 541 nm for **3** is very similar to that found for free ligand L in terms of position and band shape. Therefore, it is assigned to a silver(I)-perturbed intraligand transition. Perhaps, the two higher energy emission bands with weaker intensities, indicative of a slight modification in the photoluminescent activity in **3**, could be ascribed tentatively to either ligand-to-metal (LMCT) or metal-to-ligand charge-transfer transitions (MLCT), but further exact assignments have not carried out. Notably, free ligand L and its Ag^I complex **3** display useful photoluminescent activity in the blue/green region.

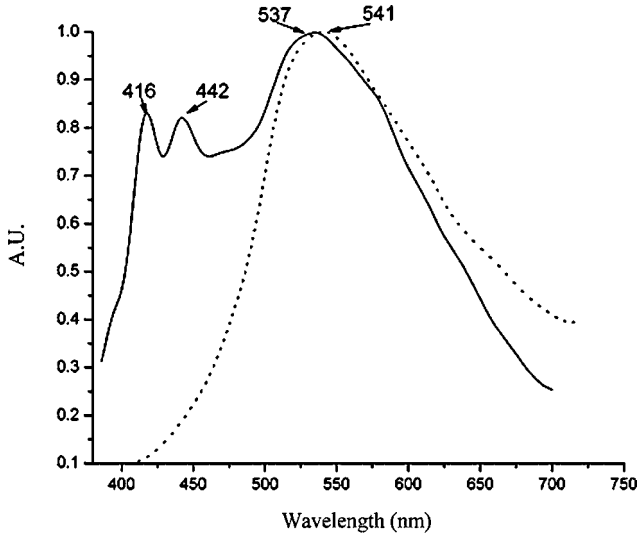

Figure 5. Fluorescence spectra of ligand L excited at 370 nm (dotted line) and complex **3** excited at 365 nm (solid line) in the solid state at room temperature.

Conclusions

We have synthesized flexible ligand L [L = 1,3-bis(4-pyridylthio)propan-2-one] and its three new coordination polymers $\{[Ni(L)_2Cl_2]\}_\infty$ (**1**), $\{[Co(L)_2(SCN)_2]\cdot(DMF)_2\}_\infty$ (**2**) and $\{[AgL]NO_3\}_\infty$ (**3**). Assemblies of L with four-connected square-planar nodes Ni^{II} and Co^{II} lead to two 3D interpenetrating nets with distinct topologies due to the metal-assisted conformational selectivity and unique combinations of ligand L around the metal centers. In **3**, L only presents a typical conformation, with higher steric energy, that links linear nodes Ag^I, leading to a 1D U-like chain, where counter-anions template both the architecture of the polymer and the A2-typical conformation of L. Clearly, L presents conformational lability that can be utilized in metal-assisted assemblies to affect the coordination architectures. Magnetic studies on complexes **1** and **2** show that the long, unconjugated ligand L is unfavorable for the electronic interactions needed for efficient superexchange between paramagnetic metal centers. Interestingly, complex **3** displays unusual fluorescent emission with multiple bands in the blue/green region. Moreover, as the ketone group incorporated into the ligand will functionalize the resultant architecture, further exploitation of such ligands in crystal engineering and material is underway.

Experimental Section

WARNING! Although we experienced no problems in handling these perchlorate compounds, they should be treated with great caution due to their potential for explosion.

General Remarks: All materials, reagents and solvents were purchased from commercial sources and used as received. Elemental

Table 1. Crystal data and structure refinement for **1**–**3**.

	1	**2**	**3**
Empirical formula	$C_{26}H_{24}Cl_2N_4NiO_2S_4$	$C_{34}H_{38}CoN_8O_4S_6$	$C_{13}H_{12}AgN_3O_4S_2$
Formula mass	682.34	874.01	446.25
Temperature [K]	293(2)	130(2)	293(2)
Crystal system	orthorhombic	monoclinic	orthorhombic
Space group	*Ibca*	*C*2/*c*	*Pnma*
a [Å]	18.447(11)	22.65(4)	5.5447(5)
b [Å]	15.952(8)	16.34(2)	14.5664(15)
c [Å]	21.40(2)	12.57(5)	22.6241(22)
α [°]	90.00(0)	90.00(0)	90.00(0)
β [°]	90.00(0)	118.60(4)	90.00(0)
γ [°]	90.00(0)	90.00(0)	90.00(0)
V [A^3]	6297(8)	4086(18)	1827.3(0)
Z, $\rho_{calcd.}$ [Mg m^{-3}]	8, 1.439	4, 1.421	4, 1.622
μ (Mo-K_α) [mm^{-1}]	1.081	0.774	1.351
θ range [°]	2.54 to 22.50	1.61 to 22.50	3.60 to 22.50
Goodness-of-fit on F^2	0.974	1.090	1.301
*R*1, *wR* [$I > 2\sigma(I)$]	0.0944, 0.2329	0.0709, 0.1933	0.0660, 0.1578
(all data)	0.1372, 0.2728	0.0737, 0.1959	0.0695, 0.1601

Table 2. Selected bond lengths [Å] and angles [°] for **1**–**3**.

Complex **1**			
Ni1–N1	2.128(8)	Ni1–N1A	2.128(8)
Ni1–N2	2.123(8)	Ni1–N2A	2.123(8)
Ni1–Cl1	2.398(3)	Ni1–Cl1A	2.398(3)
N2–Ni1–N1	87.8(3)	N1–Ni1–N1A	92.4(5)
N2–Ni1–N2A	92.1(5)	N2A–Ni1–N1A	87.8(3)
N1–Ni1–Cl1A	90.1(2)	N1A–Ni1–Cl1	90.1(2)
N2–Ni1–Cl1A	91.2(2)	N2A–Ni1–Cl1A	89.3(2)
N1–Ni1–Cl1	89.5(2)	N1A–Ni1–Cl1A	89.5(2)
N2–Ni1–Cl1A	89.3(2)	N2A–Ni1–Cl1	91.2(2)
N2A–Ni1–N1	179.4(3)	N2–Ni1–N1A	179.4(3)
Cl1A–Ni1–Cl1	179.33(17)		
Complex **2**			
Co1–N1	2.210(5)	Co1–N1A	2.210(5)
Co1–N2	2.165(6)	Co1–N2A	2.165(6)
Co1–N3	2.087(6)	Co1–N3A	2.087(6)
N2–Co1–N1	88.7(2)	N3–Co1–N1	91.5(2)
N3–Co1–N2	89.7(3)	N3–Co1–N2A	90.3(3)
N3A–Co1–N2A	89.7(3)	N3A–Co1–N2	90.3(3)
N3–Co1–N1A	88.5(2)	N3A–Co1–N1A	91.5(2)
N2A–Co1–N1A	88.7(2)	N2–Co1–N1A	91.3(2)
N3A–Co1–N1	88.5(2)	N2A–Co1–N1	91.3(2)
N1A–Co1–N1	180.0(3)	N2A–Co1–N2	180.0(3)
N3–Co1–N3A	180.0(2)		
Complex **3**			
Ag1–N1	2.151(7)	Ag1–N1A	2.151(7)
N1A–Ag1–N1	180.0(3)		

Symmetry codes: A = ½ –*x*, *y*, –*z* for **1**; A = ½ –*x*, ½ –*y*, –*z* for **2**; A = –*x*, 1 –*y*, –*z* for **3**.

analyses were determined on an Elementary Vario ELIII elemental analyzer. IR spectra were measured as KBr pellets on a Nicolet Magna 750 FT-IR spectrometer in the range 400–4000 cm^{-1}. The NMR spectrum was recorded on a Varian Inova-500 spectrophotometer at room temperature and chemical shifts are quoted in δ (ppm) relative to the deuterated solvent used. Fluorescent spectra were measured with an Edinburgh FL-FS90 TCSPC system. Temperature-dependent magnetic measurements were determined on a Quantum Design SQUID-XL7 magnetometer.

Synthesis of 1,3-Bis(4-pyridylthio)propan-2-one (L): L was synthesized under nitrogen. Sodium methylate (0.540 g, 10 mmol) and 4-pyridinethiol (1.11 g, 10 mmol) were vigorously stirred in MeOH (50 mL) for 1 h before a quantitative amount of 1,3-dichloro-2-propanone (0.635 g, 5 mmol) was added. The resulting solution was heated at 60 °C for 12 h and then filtered after cooling to room temperature. Removal of the solvent from the resultant red filtrate gave a brown oil that afforded yellow needle crystals after recrystallization from warm water. The crystalline product was redissolved in warm water (20 mL) and neutralized with $NaHCO_3$ powder. The so-obtained pale yellow precipitate was filtered off, washed with cold water and a little methanol, and then dried in air to give 0.773 g (2.80 mmol) of L (56%). $C_{13}H_{12}N_2OS_2$ (276.4): calcd. C 56.50, H 4.38, N 10.14, S 23.20; found: C 56.42, H 4.35, N 10.00, S 23.05. ^{1}H NMR (500 MHz, [D$_6$]DMSO): δ = 8.481 [d, *J* (HH) = 6.0 Hz, 4 H, H^{2,6}py], 7.519 [d, *J* (HH) = 5.0 Hz, 4 H,

$H^{3,5}$py], 4.594 (m, 4 H, -CH_2-) ppm. IR (KBr): $\tilde{\nu}$ = 3032 (w), 2942 (w), 1730 (vs), 1575 (vs), 1538 (s), 1482 (m), 1409 (vs), 1381 (s), 1220 (m), 1028 (s), 801 (vs), 702 (s), 497 (m) cm^{-1}.

Synthesis of $\{[Ni(L)_2Cl_2]\}_\infty$ (1): Solvothermal treatment of $NiCl_2 \cdot 6H_2O$ (0.024 g, 0.1 mmol), L (0.055 g, 0.2 mmol) and methanol (10 mL) at 80 °C for 1 day gave yellow-green prismatic crystals of **1** (0.048 g, 0.07 mmol, 70%). $C_{26}H_{24}Cl_2N_4NiO_2S_4$ (682.34): calcd. C 45.77, H 3.54, N 8.21, S 18.80; found: C 45.50, H 3.60, N 8.20, S 18.57. IR (KBr): $\tilde{\nu}$ = 3060 (w), 2916 (m), 1720 (m), 1601 (vs), 1535 (w), 1484 (s), 1417 (s), 1216 (m), 1072 (m), 806 (m), 718 (m), 502 (w) cm^{-1}.

Synthesis of $\{[Co(L)_2(SCN)_2]\cdot(DMF)_2\}_\infty$ (2): KSCN (0.019 g, 0.2 mmol) in DMF (5 mL) was added to a solution of $Co(ClO_4)_2 \cdot 6H_2O$ (0.037 g, 0.1 mmol) and L (0.055 g, 0.2 mmol) in DMF (5 mL) with stirring. The resulting mixture was stirred for 1 h and then filtered. Slow diffusion of diethyl ether (25 mL) into the blue filtrate for three weeks gave block orange crystals of **2** (0.065 g, 0.074 mmol, 74%). $C_{34}H_{38}CoN_8O_4S_6$ (874.01): calcd. C 46.72, H 4.38, N 12.82, S, 22.01; found: C 46.30, H 4.45, N 12.79, S 21.77. IR (KBr): $\tilde{\nu}$ = 3099 (w), 3059 (w), 2928 (w), 2873 (m), 2065 (vs), 1718 (w), 1664 (s), 1593 (vs), 1537 (w), 1485 (m), 1417 (m), 1221 (m), 1065 (m), 807 (m), 720 (m), 627 (w), 501 (m) cm^{-1}.

Synthesis of $\{[AgL]NO_3\}_\infty$ (3): A mixture of DMF (5 mL), methanol (5 mL) and CH_3CN (5 mL) was added dropwise along the wall of tube (50 mL) that contained a solution of $AgNO_3$ (0.017 g, 0.1 mmol) and DMF (5 mL) as the bottom layer. A solution of L (0.028 g, 0.1 mmol) and methanol (10 mL) as the top layer was then transferred into the tube in the same way. After slowly diffusing for two weeks, the mesosphere gave khaki needle crystals of **3** (0.023 g, 0.052 mmol, 52%). $C_{13}H_{12}AgN_3O_4S_2$ (446.25): calcd. C 34.99, H 2.71, N 9.42, S 14.37; found: C 35.10, H 2.64, N 9.17, S 14.50. IR (KBr): $\tilde{\nu}$ = 3091 (w), 2916 (w), 1720 (m), 1597 (s), 1535 (w), 1489 (m), 1422 (m), 1371 (vs), 1232 (m), 1114 (m), 1062 (m), 1026 (m), 806 (m), 718 (m), 636 (w), 487 (m) cm^{-1}.

X-ray Structure Determinations: Single-crystal data were collected on a Rigaku Mercury-CCD diffractometer at room temperature for **1** and **3,** and at 130 K for **2**, using graphite-monochromated Mo-K_α radiation (λ = 0.7107 Å). The structures were solved by direct methods and refined on F^2 by full-matrix least-squares procedures using the SHELXTL software suite.[50] All non-hydrogen atoms were refined anisotropically and the hydrogen atoms were treated as idealized contributions. For complex **2**, the propan-2-one groups of half L were split into two equivalent parts and the accommodated DMF solvent was treated as disordered; the maximum and minimum peaks in the final difference maps were 1.678 and –0.511 e $Å^{-3}$, respectively, and the largest residual density peak was close to the sulfur atom of SCN^-. Table 1 summarizes the crystallographic data of **1**–**3** and Table 2 lists selected bond lengths and angles. X-ray crystallographic data in CIF format for **1**–**3** have also been deposited. CCDC-247593 to -247595 (for **1**–**3)** contain the supplementary crystallographic data for this paper. These data can be obtained free of charge from The Cambridge Crystallographic Data Centre via www.ccdc.cam.ac.uk/data_request/cif.

Acknowledgments

This work was supported by grants from the National Nature Science Foundation of China and the Nature Science Foundation of Fujian Province.

[1] K. Kasai, M. Aoyagi, M. Fujita, *J. Am. Chem. Soc.* **2000**, *122*, 2140–2141.
[2] K.-W. Kim, M. G. Kanatzidis, *J. Am. Chem. Soc.* **1992**, *114*, 4878–4883.
[3] X.-H. Bu, W. Chen, S.-L. Lu, R.-H. Zhang, D.-Z. Liao, W.-M. Bu, M. Shionoya, F. Brisse, J. Ribas, *Angew. Chem. Int. Ed.* **2001**, *40*, 3201–3203.
[4] Z.-R. Qu, H. Zhao, Y.-P. Wang, X.-S. Wang, Q. Ye, Y.-H. Li, R.-G. Xiong, B. F. Abrahams, Z.-G. Liu, Z.-L. Xue, X.-Z. You, *Chem. Eur. J.* **2004**, *10*, 53–60.
[5] R. Horikoshi, T. Mochida, H. Moriyama, *Inorg. Chem.* **2001**, *40*, 2430–2433.
[6] N. Yoshida, H. Oshio, T. Ito, *Chem. Commun.* **1998**, 63–64.
[7] C.-Y. Su, Y.-P. Cai, C.-L. Chen, B.-S. Kang, *Inorg. Chem.* **2001**, *40*, 2210–2211.
[8] L. Raehm, L. Mimassi, C. Guyard-Duhayon, H. Amouri, *Inorg. Chem.* **2003**, *42*, 5654–5659.
[9] L. Carlucci, G. Ciani, P. Macchi, D. M. Proserpio, S. Rizzato, *Chem. Eur. J.* **1999**, *5*, 237–243.
[10] D. M. L. Goodgame, D. A. Grachvogel, I. Hussain, A. J. P. White, D. J. Williams, *Inorg. Chem.* **1999**, *38*, 2057–2063.
[11] J.-F. Ma, J. Yang, G.-L. Zheng, L. Li, J.-F. Liu, *Inorg. Chem.* **2003**, *42*, 7531–7534.
[12] X.-L. Wang, C. Qin, E.-B. Wang, Y.-G Li, C.-W. Hu, L. Xu, *Chem. Commun.* **2004**, 378–379.
[13] S. R Batten, A. R. Harris, P. Jensen, K. S. Murray, A. Ziebell, *J. Chem. Soc., Dalton Trans.* **2000**, 3829–3835.
[14] R. Horikoshi, T. Mochida, N. Maki, S. Yamada, H. Moriyama, *J. Chem. Soc., Dalton Trans.* **2002**, 28–33.
[15] X.-R. Meng, Y.-L. Song, H.-W. Hou, H.-Y. Han, B. Xiao, Y.-T. Fan, Y. Zhu, *Inorg. Chem.* **2004**, *43*, 3528–3536.
[16] M.-L. Tong, X.-M. Chen, B.-H. Ye, L.-N. Ji, *Angew. Chem. Int. Ed.* **1999**, *38*, 2237–2240.
[17] D. L. Reger, R. F. Semeniuc, V. Rassolov, M. D. Smith, *Inorg. Chem.* **2004**, *43*, 537–554.
[18] P. Borsting, P. J. Steel, *Eur. J. Inorg. Chem.* **2004**, 376–380.
[19] L. Mimassi, C. Guyard-Duhayon, L. Raehm, H. Amouri, *Eur. J. Inorg. Chem.* **2002**, 2453–2457.
[20] Y.-H. Liu, H.-C. Wu, H.-M. Lin, W.-H. Hou, K.-L. Lu, *Chem. Commun.* **2003**, 60–61.
[21] S. U. Son, B. Y. Kim, C. H. Choi, S. W. Lee, Y. S. Kim, Y. K. Chung, *Chem. Commun.* **2003**, 2528–2529.
[22] K. I. Na1ttinen, K. Rissanen, *Inorg. Chem.* **2003**, *42*, 5126–5134.
[23] K. A. Hirsch, S. R. Wilson, J. S. Moore, *Inorg. Chem.* **1997**, *36*, 2960–2968.
[24] D. M. Shin, I. S. Lee, Y. K. Chung, M. S. Lah, *Chem. Commun.* **2003**, 1036–1037.
[25] K. Uemura, S. Kitagawa, M. Kondo, K. Fukui, R. Kitaura, H.-Ch. Chang, T. Mizutani, *Chem. Eur. J.* **2002**, *8*, 3586–3560.
[26] C. M. Grunert, J. Schweifer, P. Weinberger, W. Linert, *Inorg. Chem.* **2004**, *43*, 155–165.
[27] O. R. Evans, W.-B. Lin, *Chem. Mater.* **2001**, *13*, 2705–2712.
[28] L. Han, M.-C. Hong, R.-H. Wang, J.-H. Luo, Z.-Z. Lin, D.-Q. Yuan, *Chem. Commun.* **2003**, 2580–2581.
[29] J. R. Black, N. R. Champness, W. Levason, G. Reid, *Inorg. Chem.* **1996**, *35*, 4432–4438.
[30] F. M. Tabellion, S. R. Seidel, A. M. Arif, P. J. Stang, *J. Am. Chem. Soc.* **2001**, *123*, 7740–7741.
[31] M.-C. Hong, W.-P. Su, R. Cao, M. Fujita, J.-X. Lu, *Chem. Eur. J.* **2000**, *6*, 437–431.
[32] M.-C. Hong, Y.-J. Zhao, W.-P. Su, R. Cao, M. Fujita, Z.-Y. Zhou, A. S. C. Chan, *Angew. Chem. Int. Ed.* **2000**, *39*, 2468–2470.
[33] Y.-J. Zhao, M.-C. Hong, D.-F. Sun, R. Cao, *J. Chem. Soc., Dalton Trans.* **2002**, 1354–1357.
[34] R.-H. Wang, M.-C. Hong, W.-P. Su, Y.-C. Liang, R. Cao, Y.-J. Zhao, J.-B. Weng, *Polyhedron* **2001**, *20*, 3165–3170.
[35] Y. Zheng, M. Du, J.-R. Li, R.-H. Zhang, X.-H. Bu, *J. Chem. Soc., Dalton Trans.* **2003**, 1509–1514.
[36] R.-Q. Zou, J.-R. Li, Y.-B. Xie, R.-H. Zhang, X.-H. Bu, *Cryst. Growth Des.* **2004**, *4*, 79–84.

[37] M. J. Frisch, G. W. Trucks, H. B. Schlegel, G. E. Scuseria, M. A. Robb, J. R. Cheeseman, J. A. Jr., Montgomery, T. Vreven, K. N. Kudin, J. C. Burant, J. M. Millam, S. S. Iyengar, J. Tomasi, V. Barone, B. Mennucci, M. Cossi, G. Scalmani, N. Rega, G. A. Petersson, H. Nakatsuji, M. Hada, M. Ehara, K. Toyota, R. Fukuda, J. Hasegawa, M. Ishida, T. Nakajima, Y. Honda, O. Kitao, H. Nakai, M. Klene, X. Li, J. E. Knox, H. P. Hratchian, J. B. Cross, C. Adamo, J. Jaramillo, R. Gomperts, R. E. Stratmann, O. Yazyev, A. J. Austin, R. Cammi, C. Pomelli, J. W. Ochterski, P. Y. Ayala, K. Morokuma, G. A. Voth, P. Salvador, J. J. Dannenberg, V. G. Zakrzewski, S. Dapprich, A. D. Daniels, M. C. Strain, O. Farkas, D. K. Malick, A. D. Rabuck, K. Raghavachari, J. B. Foresman, J. V. Ortiz, Q. Cui, A. G. Baboul, S. Clifford, J. Cioslowski, B. B. Stefanov, G. Liu, A. Liashenko, P. Piskorz, I. Komaromi, R. L. Martin, D. J. Fox, T. Keith, M. A. Al-Laham, C. Y. Peng, A. Nanayakkara, M. Challacombe, P. M. W. Gill, B. Johnson, W. Chen, M. W. Wong, C. Gonzalez, J. A. Pople, *Gaussian 03*, revision B.05; Gaussian, Inc.: Pittsburgh, PA, **2003**.

[38] D. M. Shin, I. S. Lee, Y. K. Chung, *Inorg. Chem.* **2003**, *42*, 8838–8846.

[39] D. M. Shin, I. S. Lee, Y. K. Chung, M. S. Lah, *Inorg. Chem.* **2003**, *42*, 2977–2982.

[40] N. G. Pschirer, D. M. Ciurtin, M. D. Smith, U. H. F. Bunz, H. C. Loye, *Angew. Chem. Int. Ed.* **2002**, *41*, 583–585.

[41] O. M. Yaghi, H. L. Li, T. L. Gory, *Inorg. Chem.* **1997**, *36*, 4292–4203.

[42] M. L. Tong, X. M. Chen, S. R. Batten, *J. Am. Chem. Soc.* **2003**, *125*, 16170–16171.

[43] B. Moulton, H. Abourahma, M. W. Bradner, J. J. Lu, G. J. McManus, M. J. Zaworotko, *Chem. Commun.* **2003**, 1342–1343.

[44] H. Sakiyama, R. Ito, H. Kumagai, K. Inoue, M. Sakamoto, Y. Nishida, M. Yamasaki, *Eur. J. Inorg. Chem.* **2001**, 2027–2032.

[45] G. De Munno, M. Julve, F. Lloret, J. Faus, A. Caneschi, *J. Chem. Soc., Dalton Trans.* **1994**, 1175–1183.

[46] B. L. Fei, W. Y. Sun, T. Okamura, W. X. Tanga, N. Ueyama, *New J. Chem.* **2001**, *25*, 210–212.

[47] M. L. Tong, X. M. Chen, B. H. Ye, L. N. Ji, *Angew. Chem. Int. Ed.* **1999**, *38*, 2237–2240.

[48] S. L. Zheng, M. L. Tong, S. D. Tan, Y. Wang, J. X. Shi, Y. X. Tong, H. K. Lee, X. M. Chen, *Organometallics* **2001**, *20*, 5319–5325.

[49] M. A. Omary, M. A. Rawashdeh-Omary, H. V. K. Diyabalanage, H. V. R. Dias, *Inorg. Chem.* **2003**, *42*, 8612–8614.

[50] G. M. Sheldrick, Bruker *SHELXTL-PC*, University of Göttingen, **1997**.

Received: September 01, 2004

